Production of ultracold diatomic and triatomic molecular ions of spectroscopic and astrophysical interest

B Roth, P Blythe, H Daerr, L Patacchini and S Schiller

Institut für Experimentalphysik, Heinrich Heine Universität Düsseldorf, 40225 Düsseldorf, Germany

E-mail: Bernhard.Roth@uni-duesseldorf.de

Abstract
We have produced large samples of ultracold (<20 mK) ArH^+, ArD^+, N_2H^+, N_2D^+, H_3^+, D_3^+, D_2^+, H_2D^+ and D_2D^+ molecular ions, by sympathetic cooling and crystallization via laser-cooled Be^+ ions in a linear radio-frequency trap. As technique, we used chemical reactions with sympathetically cooled noble gas atomic ions or N_2^+ and O_2^+ molecular ions. These ultracold molecules are interesting targets for high-precision measurements in fundamental physics and may open new routes for the study of state-selective chemical reactions relevant to interstellar chemistry.

1. Introduction

Translationally cold (in the millikelvin regime) molecular ions embedded inside Coulomb crystals are ideal targets for a large variety of investigations, including high-precision measurements of ro-vibrational transition frequencies, and state-selective studies of chemical reactions.

Heteronuclear diatomic ions, such as diatomic molecular hydrides, e.g., ArH^+ and ArD^+, are promising systems for high-precision laser spectroscopy and fundamental studies, such as tests of time independence of certain fundamental constants, namely particle mass ratios [1, 2]. For example, ArH^+ has several useful properties. Its electronic ground state is a $X^1\Sigma^+$ state. The nuclei have no quadrupole moment and only a single nuclear spin (1/2) is present. This yields a simple hyperfine structure of the ro-vibrational transitions [2]. Furthermore, ArH^+ has relatively large vibrational and rotational transition rates, but still small enough for enabling ultra-high spectral resolution [3]. One can drive the low-lying ro-vibrational transitions using commercially available continuous-wave laser sources, e.g. OPOs, in the mid-IR wavelength region, see [3] and references therein, or quantum cascade lasers. Using far-infrared laser spectroscopy the first determination of the electric dipole moment of a molecular ion, ArD^+,

was demonstrated with an accuracy at the few per cent level, by measuring the Zeeman effect in low-lying rotational transitions of ArH^+ and ArD^+, produced in a discharge source [4]. The use of ultracold ArH^+ ions may allow us to improve precision of such measurements. Precision measurements of one or several ro-vibrational transition frequencies over time could serve to test the constancy of the nuclear-to-electron mass ratio. A technique to perform high-precision spectroscopy on non-fluorescing ions has recently been demonstrated [5]. Another interesting perspective is to use certain ultracold heteronuclear diatomics, in $^{1,2,3}\Sigma$ or $^2\Pi$ states which are among the most frequent electronic ground states in molecules, as model systems for the implementation of schemes for internal state manipulation [3, 2]. For this purpose, molecules with a relatively simple hyperfine structure of the ro-vibrational transitions are more favourable, in order to limit the number of laser sources required for internal cooling schemes.

Being among the most abundant molecules in interstellar clouds, the chemistry of hydrogen molecular ions is relevant to astronomy. At present, the interstellar gas-phase chemistry of H_3^+ and its deuterated isotopomers is not completely understood [6, 7]. Measurements of state-specific reactions of H_3^+ via high-resolution infrared spectroscopy can provide valuable input for theories of ion–molecule gas-phase chemistry and precise calculations of molecular transition frequencies. Such measurements could so far only be performed on warm samples [8]. Ultracold ensembles of triatomic hydrogen molecular ions, possibly cooled to their ro-vibrational ground state using cryogenic techniques, could lead to improved studies. As an example, translationally ultracold molecular ions in low-lying ro-vibrational levels (populated at room temperature) could be excited to higher ro-vibrational levels (not populated at room temperature), using standard IR laser sources. Chemical reactions between state-prepared ultracold molecular ions and (state-prepared) ultracold neutral molecules, which are endothermic when the ions are in low-lying vibrational levels, but exothermic for the excited vibrational levels, could then be studied.

A powerful method for cooling molecular ions to translational temperatures in the millikelvin regime is sympathetic cooling. The translational energy of molecular ions can be reduced by interaction with directly cooled (laser-cooled) atomic ions. Under strong cooling, i.e., when the translational temperature drops to about 50 mK, the ions undergo a phase transition to an ordered state, a Coulomb crystal, characterized by well-defined sites [9–11]. Typical interparticle distances are in the range of a few tens of micrometres. This method has been applied to an increasing number of molecules (and atoms), since it overcomes the lack of closed optical transitions required for direct cooling and is independent of electric or magnetic dipole moments or the internal level structure [12, 13].

Recently, we have reported the production of ultracold molecular hydrogen ions, e.g., H_2^+, H_3^+, and their deuterated isotopomers HD^+, D_2H^+, H_2D^+ and D_2^+, via sympathetic cooling using laser-cooled Be^+ ions in a linear rf trap [13]. The molecular ions were produced by *in situ* ionization of neutral molecular gases (H_2, D_2 or HD) in the ion trap using low-energy electrons. Ion crystals of various sizes and ion species ratios were formed with the fraction of molecules exceeding 70%. Chemical reactions were involved in some of the molecule species production. Since the method used also leads to the formation of unwanted impurity ions purification was applied in order to remove those ions from the crystal [14, 13]. However, crystal purification usually also leads to partial loss of the molecular species of interest.

In this work, we demonstrate a novel, more efficient production method for the molecular hydrogen ions H_3^+, D_3^+, D_2^+, and for D^+. We use heavier atomic or molecular ions, e.g. Ar^+, Ne^+, Kr^+, N_2^+ or O_2^+, as reactants in order to produce ultracold and pure ensembles of H_3^+. The fraction of atomic to molecular ions can be controlled. The method was also applied to produce various ultracold deuterated hydrogen isotopomers, D_3^+, D_2^+ and D^+ atomic ions. Furthermore, multi-step chemical reactions were used to produce and reliably detect
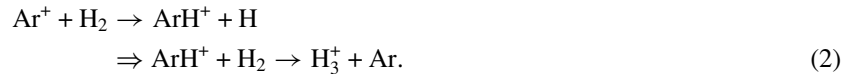
heavier medium-weight diatomic and triatomic molecular hydrides, such as ArH^+, ArD^+, N_2H^+ and N_2D^+.

2. Apparatus and methods

A detailed description of our ion trap apparatus and the basic experimental procedure is given elsewhere [11, 14]. Here, we summarize the main aspects only. We use a linear quadrupole trap to simultaneously store laser-cooled (LC) and sympathetically cooled (SC) ions. The trap is enclosed in an ultra-high vacuum chamber kept below 5×10^{-11} mbar. Stable trapping of ions is ensured by a Mathieu stability parameter, $q = 2QV_{RF}/m\Omega^2 r_0^2$, significantly below 0.9. Here, Q and m are the charge and the mass of the ions. V_{RF} and Ω are the amplitude and the frequency of the rf driving field and $r_0 = 4.3$ mm is the distance from the trap centre to the electrodes. Typically, we set the stability parameter $q \simeq 0.054$ for the Be^+ ions. In the absence of ion–ion interactions, oscillations transverse to the z-axis (the trap centreline) occur with a frequency $\omega_r = \left(\omega_0^2 - \omega_z^2/2\right)^{1/2}$, with $\omega_0 = QV_{RF}/\sqrt{2}m\Omega r_0^2$. The longitudinal frequency $\omega_z = (2\kappa QV_{EC}/m)^{1/2}$ is obtained from a static potential V_{EC} applied to the end sections of the trap in order to achieve particle confinement in the z-direction. κ is a constant determined by the trap geometry.

For laser cooling of Be^+ ions we produce light resonant with the $^2S_{1/2}(F = 2) \rightarrow {}^2P_{3/2}$ transition at 313 nm by doubly resonant sum frequency generation [15]. One of the fundamental waves is frequency stabilized to a hyperfine transition of molecular iodine. Thus, absolute frequency stability is achieved for the UV laser light. An AOM allows for shifting the UV frequency within a range of 340 MHz while maintaining absolute frequency stability. Optical pumping to the metastable ground state $^2S_{1/2}(F = 1)$ is prevented using a repumper red detuned by 1.250 GHz. The cooling laser beam is along z.

Neutral beryllium atoms are evaporated from an oven and ionized *in situ* in the trap by an electron beam crossing the trap centre. The Be^+ ions are subsequently laser-cooled so that they undergo a phase transition to an ordered state, a Coulomb crystal [16]. The phase transition is monitored using a charge-coupled device (CCD) camera and a photo-multiplier tube (PMT), both located perpendicular to the trap symmetry axis. Typically, the translational temperature of the Be^+ ions in such crystals is in the few millikelvin range [11] (see section 3 for a description of the method used for temperature determination). Then, Ar^+, Ne^+, Kr^+ or O_2^+ ions are produced by electron-impact ionization of neutral gases introduced to the vacuum chamber at pressures of $\approx 4 \times 10^{-10}$ mbar. The loading rate is controlled by the partial pressure of the neutral gas and the electron beam intensity. A fraction of the ions is sympathetically cooled and crystallized via Coulomb interaction with the ultracold Be^+ ions and embedded in ordered ion shells at larger radii compared to the Be^+ ions, due to their larger mass-to-charge ratio. After allowing for the gas pressure to drop to the initial value, neutral molecular hydrogen gas is introduced in the vacuum chamber at partial pressures of $\approx 2 \times 10^{-10}$ mbar. As a result, H_3^+ molecular ions are formed via two-step ion-neutral chemical reactions. The two reaction paths are, respectively,

$$Ar^+ + H_2 \rightarrow Ar + H_2^+$$
$$\Rightarrow H_2^+ + H_2 \rightarrow H_3^+ + H \tag{1}$$

$$Ar^+ + H_2 \rightarrow ArH^+ + H$$
$$\Rightarrow ArH^+ + H_2 \rightarrow H_3^+ + Ar. \tag{2}$$

The initial reactions in (1) and (2) are exothermic by ≈ 0.15 eV and have a branching ratio of 0.15:0.85. They are expected to proceed with a temperature-independent Langevin reaction

rate constant $k_L = 1.9 \times 10^{-9}$ cm^3 s^{-1}; see, e.g., [17–19]. For (1), to the best of our knowledge, no measured rate constant has been reported so far. The second step in (1), being exothermic by ≈ 2 eV, proceeds with a large (measured) rate constant $k = 2.9 \times 10^{-9}$ cm^3 s^{-1} [19–21].

In reaction (2), the (measured) rate constant is $k = 1.1 \times 10^{-9}$ cm^3 s^{-1}, for the first step [19], and $k = (5–9) \times 10^{-10}$ cm^3 s^{-1} for the second step, which is exothermic by ≈ 1.67 eV, [19, 18]. Similar reactions occur when Ne$^+$, Kr$^+$, N$_2^+$ or O$_2^+$ are used as reactants, with smaller (by a factor of 2 for Kr$^+$) or comparable (for N$_2^+$ and O$_2^+$) rate constants for the respective reaction paths. Furthermore, for the case of N$_2^+$ and O$_2^+$, the second reaction paths in (2) proceed with rate constants smaller (by a factor of 5–10) than the rate constants for the initial reaction paths [22, 23]. For the case of Ne$^+$, the reaction should proceed at a calculated Langevin rate $k_L = 1.53 \times 10^{-9}$ cm^3 s^{-1} (see [19] and references therein) however, no experimental results were reported to date.

The produced light diatomic and triatomic hydrogen molecular ions, H$_2^+$ and H$_3^+$, are embedded in the vicinity of the trap axis, where they displace the heavier Be$^+$ ions. A dark core is observed appearing in the crystal. Since the reaction between H$_2^+$ ions and neutral H$_2$ is relatively fast, the amount of H$_2^+$ formed (relative to H$_3^+$) can be controlled by the duration of the H$_2$ inlet. Experimentally, for sufficiently long H$_2$ inlet times (typically on the order of a few tens of seconds) one can achieve full conversion of the H$_2^+$ ions into H$_3^+$ ions.

The molecular hydrogen ions, H$_2^+$ and H$_3^+$, are identified via excitation of their trap (secular) oscillation modes and detection of the induced change in the fluorescence of the atomic coolant ions. For the measurements in this work we excited radial oscillation modes only. However, for slightly anisotropic trap potentials, leading to small mass-specific displacements of the different ion species from trap centre, a coupling between radial and axial oscillation modes is induced, as observed for some of the generated crystals. In the presence of heavier molecules outside the Be$^+$ ions, and/or in the presence of strong cooling light pressure forces on the Be$^+$ (which moves, e.g., the heavy ions to one end of the crystal) in an anisotropic trap potential, the radial excitation of the heavy ions in the outer crystal regions couples into the z-motion of the Be$^+$ ions in the following way: as the heavy ions are moved radially (even at small amplitudes, far away from their own radial motional frequency), the Be$^+$ ions are displaced along z, and so their axial motion is excited. The Be$^+$ z-resonance is not present if the heavy ions are removed from the trap. This effect has to be taken into account for the analysis the motional frequency spectra obtained.

For the radial excitation of particle oscillation modes an additional rf field is applied to an external electrode parallel with the z-axis of the trap, located between the two uppermost trap electrodes (at 45° to the x- and y-axis of the trap). When the frequency of the excitation field is resonant with a mode of an SC ion species the Be$^+$ fluorescence level changes. This can be observed via the PMT. The change is due to the fact that the SC ion species' heating also leads to a heating of the LC ions, via Coulomb interaction, and thus, to a change of the observed atomic fluorescence [24]. The trap oscillation spectra in this work were obtained with the laser detuned to the red of the cooling transition by approximately the natural line width of Be$^+$ (≈ 20 MHz). For such a detuning, the excitation of a particular SC species leads to an increase of atomic fluorescence.

For a trapped SC ion with mass m the radial oscillation frequency is approximately given by

$$\omega = \frac{m_{Be}}{m} \omega_{Be}, \qquad (3)$$

with $\omega_{Be}(m_{Be})$ being the radial oscillation frequency (mass) of the ^{9}Be$^+$ [25]. For the parameters used, $\omega_{Be} = 280$ kHz. Experimentally, an oscillating electric field with its

frequency scanned between 10 kHz and 2 MHz is applied to the plate electrode, with amplitudes of up to several volts to excite the collective motion of the ions.

The CCD camera images of the Be^+ ion fluorescence obtained are compared to the results from molecular dynamics (MD) simulations. In the simulation we solve Newton's equations of motion for LC and SC particles in an effective, time-independent harmonic potential. The simulations are performed using a simple linear viscous damping force to describe the cooling laser [26], and include light pressure forces and trap asymmetries (where required). These asymmetries, obvious from radial asymmetries of imaged ion crystals, can arise from static stray potentials leading to species-dependent displacements of the ions from trap centre. In order to allow for comparison with the observed structures the calculated ion trajectory positions are averaged over time and the obtained spatial probability distribution is plotted.

Using the MD simulations, the motional frequency spectrum for pure and mixed-species ion crystals can also be computed. In the simulation, a small (uniform) step-function perturbation is applied to all ion species in, e.g., the x-direction, and then the system is allowed to evolve, leading to damped oscillations of the ions around their equilibrium positions. The Fourier spectrum of the sum over all coordinates x is the computed motional spectrum for the case of small excitation amplitudes [27].

3. Production of ultracold diatomic and triatomic hydrogen molecular ions

3.1. H_3^+ ions

Figure 1 illustrates the production of ultracold H_3^+ ions using chemical reactions and sympathetic cooling. In the example given, Ar^+ ions were used as reactants.

First, an about 1.3 mm long Coulomb crystal containing ≈ 1250 Be^+ ions was produced, figure 1(a). The crystal displays an ordered shell structure with a typical inter-shell spacing of ≈ 29 μm. An upper limit for the translational temperature of the crystal of ≈ 10 mK was deduced from MD simulations. For this purpose, the size of the imaged ion spots was compared to the simulations. The estimated temperature agrees well with direct temperature measurements based on the determination of the spectral line shape of the spontaneous emission fluorescence; see [11, 25].

Subsequently, Ar^+ ions, produced *in situ* in the trap, were sympathetically crystallized and embedded in shells located at larger radii compared to the Be^+ ion shells, due to their larger mass-to-charge ratio. This leads to a massive radial deformation of the Be^+ ion shells, due to space-charge effects, figure 1(b). Since the camera images show a projection of the ion crystal perpendicular to its symmetry axis (along z) the deformation of the Be^+ shells becomes obvious on the upper and lower part of the image only. The longitudinal extension of the crystal is significantly increased, exceeding the field of view of the CCD camera. According to the MD simulations, the crystal has an estimated length of ≈ 3 mm and contains around 1000 Ar^+ ions. The crystal shape is consistent with small admixtures of lighter impurities (≈ 150 ions), such as N_2^+ and Ar^{++}, formed by chemical reactions or electron-impact ionization of background gas molecules during loading (see also the secular excitation spectrum in figure 2(a)). The SC ion temperature is estimated at ≈ 20 mK, from the simulations and assuming thermal equilibrium with the Be^+ ions. Usually, Be^+ ion losses are small during the loading of Ar^+. The slight asymmetry of the crystal along the z-axis (in longitudinal direction) is due to light pressure forces felt by the atomic coolants only.

In the next step, ultracold H_3^+ ions are formed via the chemical reactions (1) and (2), as evidenced by the appearance of a large dark crystal core, figure 1(c) (see below for the mass-spectroscopic analysis of the ions formed). Note that the small dark core on the left part
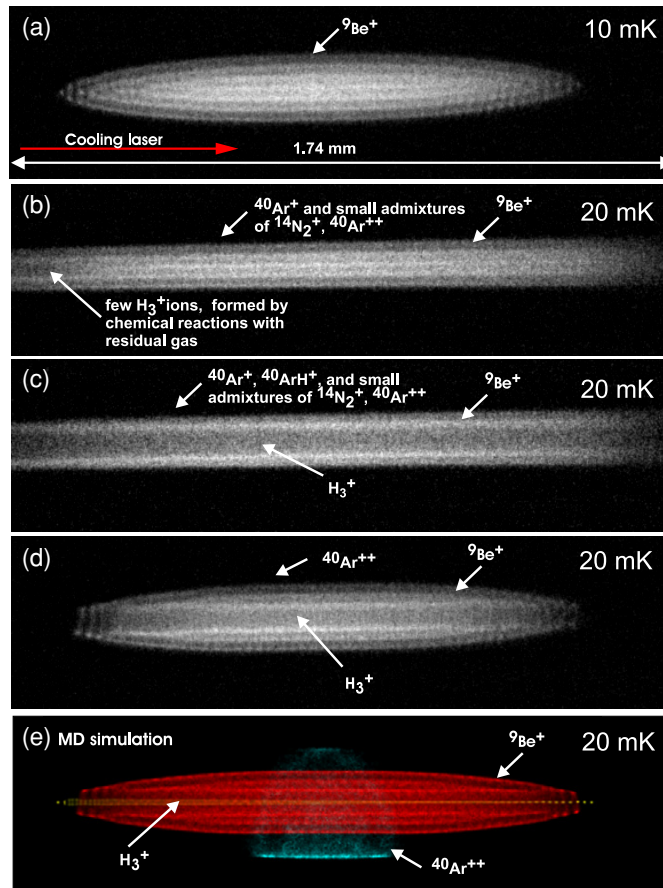
Figure 1. (a) Fluorescence image of a pure Be^+ ion crystal, (b) after loading with Ar^+ ions, (c) after H_2 inlet, showing formation of H_3^+ ions via chemical reactions, (d) after removal of Ar^+, ArH^+ and heavier contaminants, by trap opening and re-closing. We deliberately did not remove Ar^{++} ions. The cooling laser beam direction is to the right. Camera integration time was 2 s. Estimates of the translational temperatures, obtained from MD simulations, are indicated. (e) MD simulation of a large multi-component ion crystal containing ≈1150 Be^+ ions, ≈100 H_3^+ ions and ≈30 Ar^{++} ions at ≈20 mK. The shape of the simulated crystal is in good agreement with the crystal in (d).

(This figure is in colour only in the electronic version)

of the crystal in figure 1(b) is also due to H_3^+ ions formed via chemical reactions between Ar^+ and background hydrogen molecules, as found via secular mass-spectroscopy. Furthermore, ArH^+ was formed, as described in section 4.

Usually, chemical reactions between laser-excited Be^+ ions and neutral H_2 gas occur, leading to the formation of BeH^+, and thus, to loss of Be^+ ions [28]. However, this process was minimized here by reducing the population in the excited state of Be^+ by strongly detuning the laser frequency to the red of the cooling transition during exposure of the crystal to neutral H_2. The absence of BeH^+ is also confirmed by MD simulations [25].

The third step consists in the removal of ions with a mass-to-charge ratio larger than ≈20 from the trap. This is achieved by applying a sufficiently large static quadrupole potential to the central trap electrodes. The symmetry of the trap secular potential is broken to the point that the motion of the ions becomes unstable in one radial direction for heavy ions but
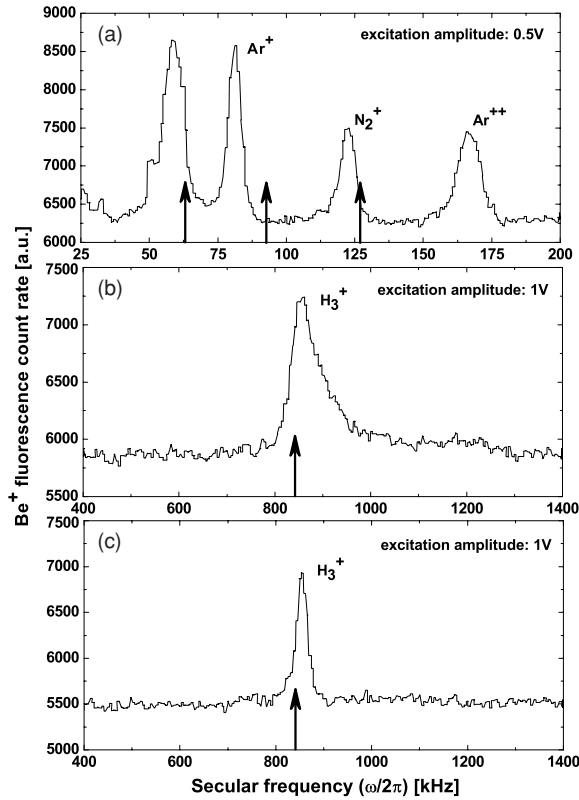
Figure 2. Motional frequency spectra for multi-species crystals: (a) after loading of Ar^+ ions (figure 1(b))—sweep direction is towards higher frequencies; (b) after inlet of H_2 and formation of ultracold H_3^+ ions (figure 1 c); (c) after the removal of ions heavier than Ar^{++} (figure 1(d)). The calculated single-particle secular frequencies are marked as arrows: Ar^+, 63 kHz; N_2^+, 90 kHz; Ar^{++}, 126 kHz; H_3^+, 840 kHz. The strong deviations between observed and calculated motional frequencies occur in these (large) ion crystals, due to the Coulomb interaction between the ions.

not for the lighter SC species and the coolants [14]. In the example shown, we deliberately did not remove impurities with a mass-to-charge ratio smaller than ≈ 20, mostly Ar^{++}, from the crystal, in order to estimate their number via the MD simulations. Figure 1(d) shows the resulting ion crystal. This crystal can be well reproduced by the MD simulations, figure 1(e), if the number of Be^+ ions ≈ 1150, the number of molecular hydrogen ions ≈ 100, the (assumed uniform) translational temperature of the (multi-species) ion crystal is 20 mK, and the number of Ar^{++} ions is 30.

In general, the number of H_3^+ ions can be controlled by the pressure of the neutral hydrogen gas and the loading time, and can be varied over a wide range, from a few ions embedded as a string on the crystal axis up to a few thousand ions forming a large dark core. For the production of small numbers of ultracold H_3^+ it is important that the residual gas partial pressure of molecular hydrogen is sufficiently low.

3.2. Detection via secular excitation mass spectroscopy

Figures 2(a)–(c) show the measured secular excitation mass spectra obtained for the crystals of figures 1(b)–(d). The secular excitation spectrum of the ion crystal after loading with Ar^+ is

presented in figure 2(a). The spectrum shows a fairly complicated structure with pronounced features at 58 kHz, 82 kHz, 122 kHz and 166 kHz. The calculated single-particle secular frequencies for Ar^+, N_2^+ and Ar^{++} are 63 kHz, 90 kHz and 126 kHz. Due to Coulomb coupling between the ions the measured frequencies deviate significantly from the calculated single-particle frequencies; see, e.g., [30, 29]. Therefore, the MD simulations are used for assigning the resonances to the various species.

The feature at 58 kHz can be attributed to the excitation of the axial ω_z Be^+ mode. This feature appears to be split in frequency, as indicated in figure 2(a), caused by small anisotropies of the trap secular potential. The feature at 82 kHz is due to sympathetically crystallized Ar^+, whereas the features at 122 kHz and 166 kHz are attributed to N_2^+ and Ar^{++} ions, respectively. As a check, measurements in the cloud state, where coupling between ions is weak, yield secular frequencies that agree within the experimental resolution with the calculated values.

Figure 2(b) shows the secular spectrum of the crystal after exposure to neutral H_2 gas. It shows the low mass-to-charge region indicating the content of the produced dark crystal core. The spectrum shows an asymmetric feature with a maximum at $\approx$855 kHz, attributed to the production of translationally ultracold H_3^+ ions. After the removal of the outer (heavy) SC particles, ArH^+, Ar^+, N_2^+, but not Ar^{++}, the feature has narrowed and become symmetric (figure 2(c)). According to the MD simulations, the change in the width can be explained by space-charge effects induced by the heavier SC ions located outside the Be^+ shells. This interpretation is also consistent with the strong deformation of the crystal shape following the loading with neutral argon gas. In addition, an increased translational temperature of the crystal (due to the embedded SC particles) or temperature gradients in radial and axial trap direction could contribute to the broadening of the H_3^+ secular line shown in figure 2(b).

For comparison, the secular frequency spectrum of another Be^+ ion crystal of comparable size and shape after inlet and electron beam ionization of neutral H_2 gas is presented in figure 3(a). The corresponding secular frequency spectrum typically shows a broad feature originating from embedded H_3^+ and H_2^+ ions with their trap modes of oscillation being strongly coupled. Repeated secular excitation leads to ejection of a part of the SC particles from the trap and, thus, to weaker coupling between the different species. Then, the individual contributions of H_3^+ and H_2^+ modes can be resolved, as shown in figure 3(b). The spectrum then exhibits two broad features with maxima at $\approx$800 kHz and $\approx$1170 kHz. The width of the two features and their shift from the single-particle frequencies of 840 kHz $\left(H_3^+\right)$ and 1260 kHz $\left(H_2^+\right)$ are due to the large excitation amplitude used and, again, due to Coulomb coupling between the ions.

The computed motional frequency spectrum for the two-component ion crystal shown in figure 1(b), containing $\approx$1100 Be^+, $\approx$1300 Ar^+, and small admixtures of N_2^+ ($\approx$150) and Ar^{++} ions ($\approx$150), is presented in figure 4. This spectrum shows three features at around 75 kHz, 126 kHz and 170 kHz, stemming from embedded Ar^+, N_2^+ and Ar^{++} ions, respectively. The features in the simulated spectrum agree with the measured data (figure 2(a)) at the level of a few kilohertz, which is the typical level of agreement between our simulations and the measurements. However, the position of the double feature at around 40 kHz, attributed to the excitation of the axial (ω_z) Be^+ mode and split in frequency due to the anisotropy of the trap secular potential (reproduced in the simulations), and the position of the feature at 75 kHz are shifted to lower values compared to the measured frequencies. This shift might be explained by nonlinearities in the response signal, since in the simulations the perturbation amplitude applied is small compared to the amplitude applied in experiment. Furthermore, the features at 126 kHz and at 170 kHz are shifted towards (slightly) larger values compared to the measured data, which is attributed to the different excitation amplitudes together with space-charge effects [27]. The smaller features at frequencies <25 kHz are numerical artefacts.
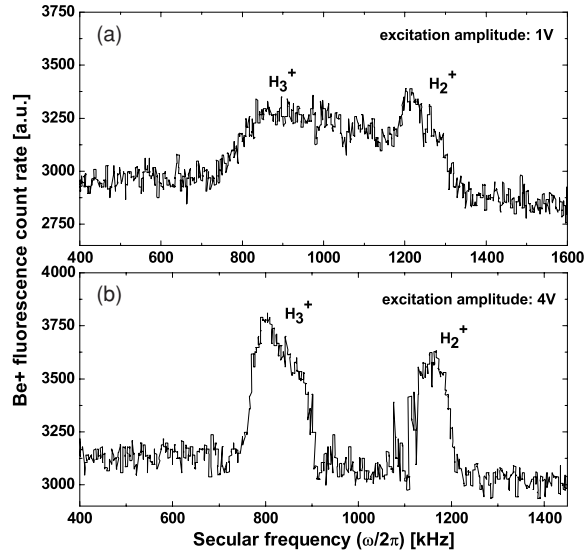
Figure 3. Motional frequency spectra for a Be^+ crystal after (a) loading of H_2^+ and H_3^+ via electron-impact ionization of neutral H_2. The spectrum shows a broad feature between 857 kHz and 1300 kHz, with maxima indicated around 850 kHz and 1200 kHz, originating from SC H_3^+ and H_2^+ ions, in approximately equal numbers, and the coupling between their trap modes of oscillation. This interpretation is confirmed by our MD simulations, (b) after repeated secular excitation where some of the SC particles were removed using a larger excitation amplitude (4 V).
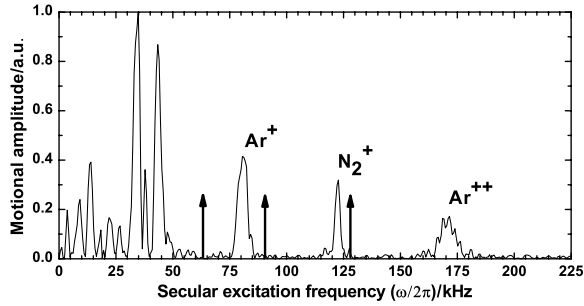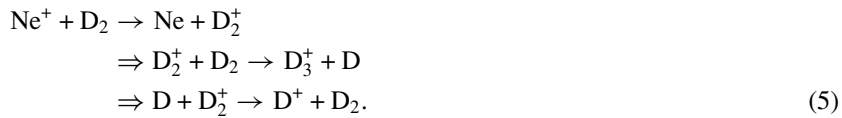

Figure 4. MD simulation of the motional frequency spectrum of the crystal shown in figure 1(b). The single-particle secular frequencies for Ar^+ (63 kHz), N_2^+ (90 kHz) and Ar^{++} (126 kHz) are marked with arrows. The double feature at around 40 kHz originates from the excitation of the axial ω_z Be^+ trap mode, whereas the smaller features at frequencies <25 kHz are numerical artefacts.

3.3. D_3^+, D_2^+ and D^+ ions

Figure 5 illustrates that the method described can also be used to produce samples of ultracold D_3^+, D_2^+ and D^+ ions. The relevant chemical reactions are
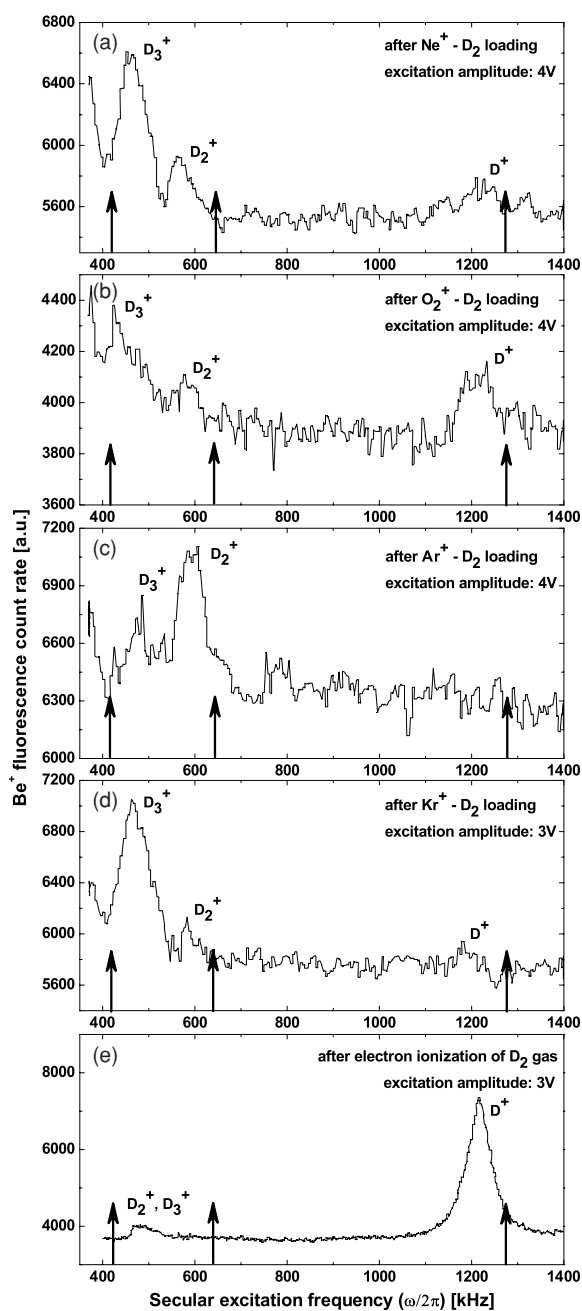
$$Ne^+ + D_2 \rightarrow NeD^+ + D$$
$$\Rightarrow NeD^+ + D_2 \rightarrow D_3^+ + Ne \qquad (4)$$
$$Ne^+ + D_2 \rightarrow Ne + D_2^+$$
$$\Rightarrow D_2^+ + D_2 \rightarrow D_3^+ + D$$
$$\Rightarrow D + D_2^+ \rightarrow D^+ + D_2. \qquad (5)$$

Figure 5. Spectrum of a Be^+ ion crystal after loading of (a) Ne^+ ions and D_2 inlet, (b) O_2^+ ions and D_2 inlet, (c) Ar^+ ions and D_2 inlet, (d) Kr^+ ions and D_2 inlet. Sweep direction is towards higher frequencies. (e) loading and electron-impact ionization of neutral D_2; excitation amplitude: 3 V. The single-particle secular frequencies are marked by arrows: D_3^+, 420 kHz; D_2^+, 640 kHz; D^+, 1260 kHz.

Whereas the first step of reaction (4) should proceed at a (calculated) Langevin reaction rate of $k_L = 1.53 \times 10^{-9}$ cm^3 s^{-1}, for the second step smaller values for the rate constant were

measured, $k = 2 \times 10^{-11}$ cm^3 s^{-1} [19]. The second step in reaction (5) occurs with a rate constant $k = 1.5 \times 10^{-9}$ cm^3 s^{-1}, whereas for the third step, exothermic by $\approx$1.87 eV, $k = 5 \times 10^{-10}$ cm^3 s^{-1} [31].

Figure 5(a) shows the motional frequency spectrum of a crystal after loading of Ne$^+$ ions and leaking in neutral D$_2$ gas for several seconds. The spectrum displays three features at frequencies of 460 kHz, 560 kHz and 1220 kHz. The first two features are attributed to the presence of ultracold D$_3^+$ and D$_2^+$ molecules. Again, the measured frequencies deviate significantly from the single-particle motional frequencies, 420 kHz $\left(D_3^+\right)$ and 640 kHz $\left(D_2^+\right)$, respectively, due to Coulomb coupling. The shift of the D$_2^+$ line is larger since the relative fraction of D$_3^+$ to D$_2^+$ ions is $\approx$3. The third (smaller) feature is attributed to the presence of small amounts of D$^+$ ions (single-particle frequency: 1260 kHz). The rise of the PMT count rate at $\approx$380 kHz is due to the onset of the excitation of the Be$^+$ trap oscillation mode (280 kHz).

The chemical reactions occurring differ significantly when using O$_2^+$ and Ar$^+$ as reactants, whereas when using Kr$^+$ ions they proceed similar to the case with Ne$^+$. Figure 5(b) shows a secular frequency spectrum of a Be$^+$-O$_2^+$ ion crystal after leaking in neutral D$_2$ gas. The resulting ultracold ion plasma contains three SC particle species, D$_3^+$, D$_2^+$ and D$^+$, at an approximately equal concentration. Ar$^+$ as a reactant mainly produces D$_3^+$ and D$_2^+$ ions; see figure 5(c). Finally, with Kr$^+$ the main fraction is D$_3^+$; figure 5(d). Note that for the formation of D$^+$ ions a three-step chemical reaction is required.

For comparison, figure 5(e) shows a typical secular frequency spectrum following inlet and electron-impact ionization of D$_2$ gas. The spectrum shows a large feature at 1220 kHz, originating from the D$^+$ ions formed, and a second, much smaller feature at $\approx$480 kHz, originating from D$_3^+$ and D$_2^+$ ions. Its frequency lies between the single-particle values for D$_3^+$ and D$_2^+$, due to the strong coupling between the two species. Typically, mixtures of D$_3^+$, D$_2^+$ and D$^+$ ions are produced, with their relative fractions varying with D$_2$ loading time and electron beam energy.

4. Production of nitrogen hydride and argon hydride molecular ions

4.1. N$_2$H$^+$ and N$_2$D$^+$ ions

Ultracold N$_2$H$^+$ and N$_2$D$^+$ molecular ions were produced via the reactions

$$N_2^+ + H_2 \rightarrow N_2H^+ + H \tag{6}$$
$$N_2^+ + D_2 \rightarrow N_2D^+ + D. \tag{7}$$

If the H$_2$ or D$_2$ gas is removed sufficiently early multi-step reactions of the type (2) and (4) do not occur efficiently, and the molecular ions remain in the trap.

The detection of (small) amounts of nitrogen hydride (or argon hydride) molecular ions via secular excitation mass spectrometry in the crystal state is complicated mainly due to the limited experimental resolution and the coupling between LC and SC particles which depends on the number of ions involved, their translational temperature and the excitation amplitude. This can lead to combined trap modes of oscillation in the spectra, as illustrated in figure 6. There, an ensemble of H$_2^+$ and H$_3^+$ ions, with its secular spectrum shown in figure 6(a), was exposed to molecular nitrogen gas and the secular spectrum was recorded after the observed dark crystal core, stemming from embedded H$_2^+$ and H$_3^+$ ions, disappeared completely, figure 6(b). The spectrum shows two broad features at around 30 kHz and 120 kHz, attributed to the interplay between trap oscillation modes of Be$^+$ and N$_2$H$^+$ ions formed via chemical reactions.
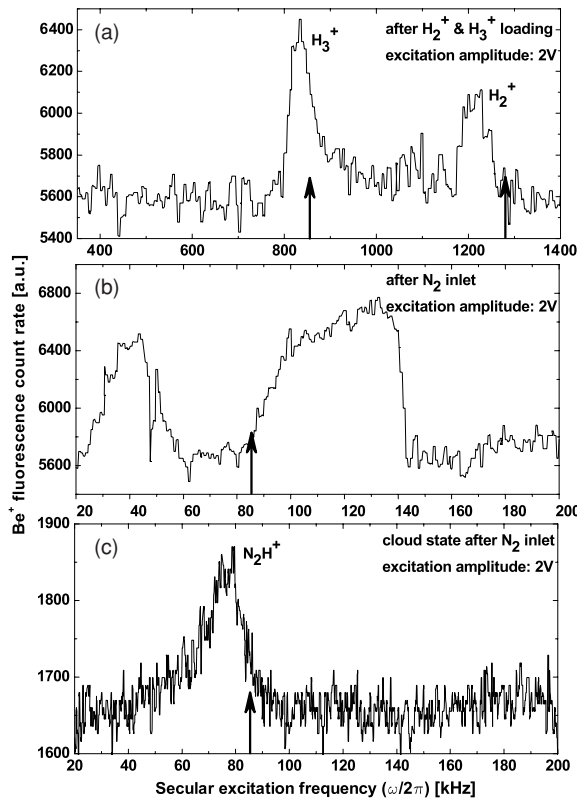
Figure 6. Motional frequency spectrum for a Be$^+$ ion crystal after inlet and electron-impact ionization of H$_2$ gas (a), after subsequent inlet of neutral N$_2$ in the crystal state (b), and in the cloud state (c). Arrows as before.

The N$_2$H$^+$ feature is hidden in the broad structure at around 120 kHz. In the cloud state secular spectrum, figure 6(c), the composite trap modes of oscillation disappear, due to a weaker coupling, and a single feature is observed, stemming from N$_2$H$^+$. However, it is desirable to detect the molecular ions formed in the crystal state, in order to estimate their number and their translational temperature by the simulations. For this purpose and in order to avoid complications originating from coupling effects in strongly correlated plasmas, a different detection technique was developed. An additional chemical reaction is introduced, in order to shift the resonance frequency of the reaction products formed in this step to an experimentally more favourable frequency region and still allow for an unambiguous identification of the molecular ions formed in the first step.

The production and detection of ultracold N$_2$H$^+$ molecular ions is shown in figure 7. First, N$_2^+$ (and smaller amounts of N$^+$ ions) were produced and embedded in the crystal. Figures 7(a) and (b) show the measured motional frequency spectra for the multi-species ion plasma in the crystal and the cloud state, respectively. Due to Coulomb coupling, the motional frequencies deviate significantly between the two states. Furthermore, the feature at around 40 kHz, originating from the excitation of the axial Be$^+$ mode, is absent in the cloud state spectrum, probably due to a weaker coupling between radial and axial trap modes of different ion species, as explained above. After inlet of neutral H$_2$ gas, hydrogen molecular ions, H$_3^+$
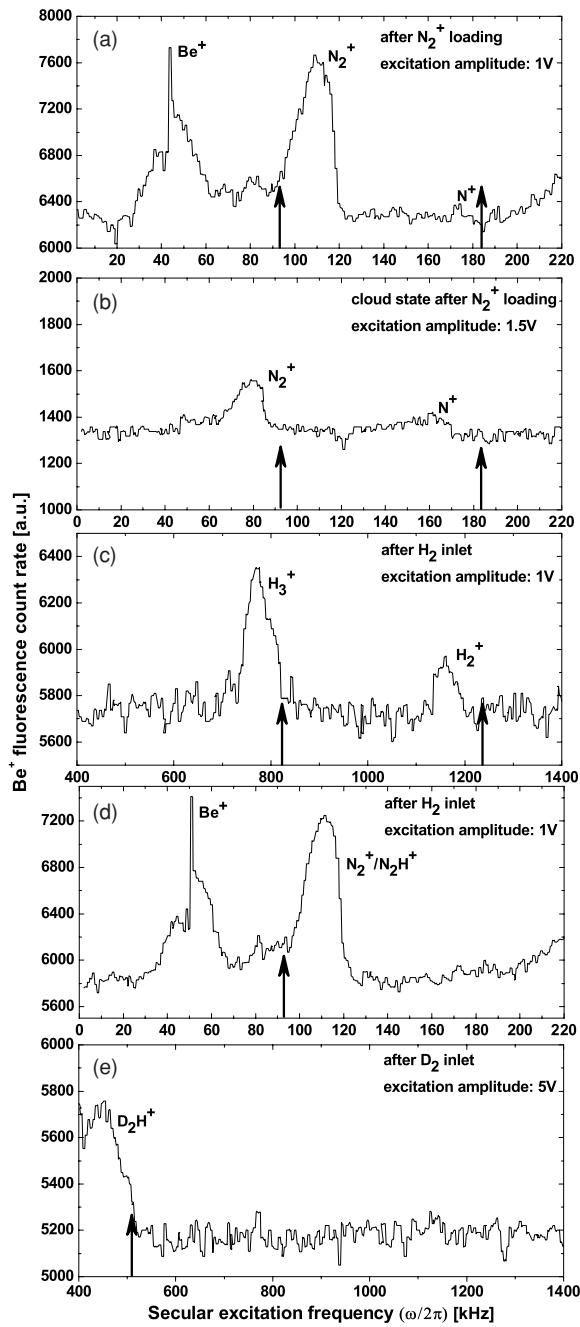
Figure 7. Motional frequency spectra for a Be^+ ion ensemble after inlet and electron-impact ionization of N_2 gas (a), (b), after subsequent inlet of neutral H_2, for the low-mass range (c) and the high-mass range (d), and followed by inlet of neutral D_2 (e). Part (b) is for the cloud state, and parts (a), (c)–(e) are for the crystal state. Arrows as before.

and H_2^+, are produced; see reactions (4) and (5). The corresponding secular spectrum is shown in figure 7(c), with the size of the N_2^+ feature, now containing also N_2H^+, reduced during the
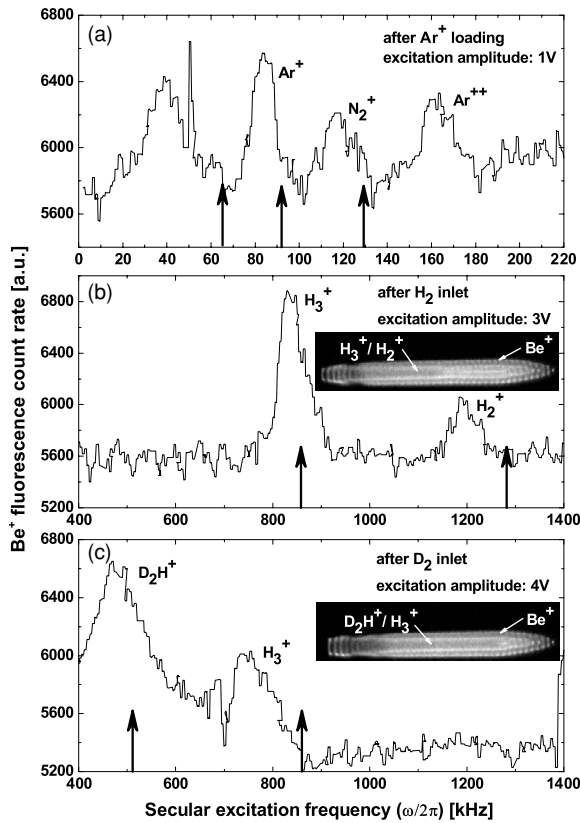
Figure 8. Motional frequency spectrum for a Be^+ ion crystal after inlet and electron-impact ionization of Ar gas (a), after subsequent inlet of neutral H_2 (b), and additional inlet of neutral D_2 (c). Arrows as before.

above reactions, figure 7(d). In the next step, exposure of the ion crystal to neutral D_2 leads to the appearance of a mass-5 feature in the spectrum, figure 7(e), attributed to the formation of ultracold D_2H^+ ions via

$$N_2H^+ + D_2 \rightarrow D_2H^+ + N_2. \tag{8}$$

The dark crystal core formed in the first step (containing H_3^+ and H_2^+) increases during the second step (D_2 inlet) indicating the formation of additional ultracold molecules, D_2H^+. The appearance of a mass-5 feature in the spectrum cannot be explained via other reaction channels, therefore, this allows for identification of the species produced as D_2H^+. Analogously, ensembles of ultracold N_2D^+ molecules were formed and detected via the appearance of a mass-4 feature in the spectrum. MD simulations were used to deduce an upper limit for the translational temperature of the nitrogen hydride molecules. The observed ion crystal structure can be reproduced in the simulations when the translational temperature of the nitrogen hydride ions is at below 20 mK. Therefore, we can conclude that the molecules formed are in the crystal state.

4.2. ArH⁺ ions

Figure 8(a) shows the motional frequency spectrum after inlet and electron-impact ionization of Ar gas. In addition to a double feature at around 40 kHz, originating from the excitation

of the axial Be^+ trap mode, the spectrum displays three distinct features, originating from embedded Ar^+ (at around 85 kHz), doubly charged Ar^{++} (at around 160 kHz), and N_2^+ from residual gas (at around 115 kHz). After subsequent H_2 inlet, in the secular spectrum, the presence of ArH^+ produced via reaction (2) cannot be resolved. The low-mass spectrum evidences the appearance of a dark crystal core which is due to the formation of ultracold H_3^+ and H_2^+ ions via reactions (1) and (2); figure 8(b). Typically, the H_2 inlet is stopped after a few seconds, when the longitudinal extension of the dark crystal core is approximately half the total crystal extension; see the inset of figure 8(b) (longer exposure times would lead to larger crystals cores and thus more molecular hydrogen ions formed, an unfavourable situation for the detection method described below).

The production of ArH^+ in the previous step can be shown by a subsequent exposure to neutral D_2 gas. ArH^+ ions will further react via the exothermic (by ≈ 1.67 eV) reaction,

$$ArH^+ + D_2 \rightarrow D_2H^+ + Ar, \tag{9}$$

leading to the formation of mass-5 molecular ions, D_2H^+; see figure 8(c). During this reaction, the dark Be^+ crystal core, initially containing H_3^+ and H_2^+ only, increases in size showing that additional light molecules are formed and embedded around the crystal axis; see the inset of figure 8(c).

The D_2H^+ formation paths are

$$H_2^+ + D_2 \rightarrow D_2H^+ + H \tag{10}$$
$$H_3^+ + D_2 \rightarrow D_2H^+ + H_2, \tag{11}$$

where H_2^+ and H_3^+ are ions in the core. The rate constant for the first reaction is $k = 3.2 \times 10^{-9}$ cm^3 s^{-1} [32], and for the second reaction $k = 1.2 \times 10^{-9}$ cm^3 s^{-1} can be assumed; see [33]. These reactions would not increase the number of ions in the core, as the produced D_2H^+ would, at best, replace a H_2^+ or H_3^+ core ion. Thus, the increase of the core size can only be explained by the presence of ArH^+.

As reactions (1) and (2) proceed at only slightly larger Langevin rates compared to reactions (4) and (5) (see [19]) residual Ar^+ is still contained in the crystal after the H_2 inlet, so that D_2 inlet will then lead to the formation of mass-6 (D_3^+), mass-4 (D_2^+) and mass-2 ions (D^+) via reactions (4) and (5), but not to mass-5 ions, D_2H^+. These ions are not observed in the spectrum, probably because of the domination of the large D_2H^+ feature. Similarly, reactions between N_2^+ or Ar^{++} contaminants and neutral D_2 would also not lead to the formation of mass-5 ions.

4.3. ArD$^+$ ions

The formation of ultracold ArD^+ ions is illustrated in figure 9. Here, ultracold Ar^+ ions (and smaller numbers of N_2^+ contaminants), embedded in a Be^+ ion crystal, were exposed to neutral D_2, leading to the formation of ArD^+ and D_2^+ ions via reaction (4). The secular spectrum (figure 9(b)) shows a pronounced feature at around 580 kHz, attributed to the presence of D_2^+, and a smaller feature at around 800 kHz, originating from H_3^+ ions formed by chemical reactions of Ar^+ with residual H_2 gas via reactions (1) and (2). Subsequent exposure of the ions to H_2 gas leads to the formation of additional mass-4 ions, H_2D^+, via

$$ArD^+ + H_2 \rightarrow H_2D^+ + Ar, \tag{12}$$

as evidenced by the increase in size of the mass-4 peak and the observed increase in the size of the crystal core. The rate constant for this reaction is $k = 9.9 \times 10^{-10}$ cm^3 s^{-1} [18]. All other competing reaction channels, see reactions (1) and (2), would lead to the
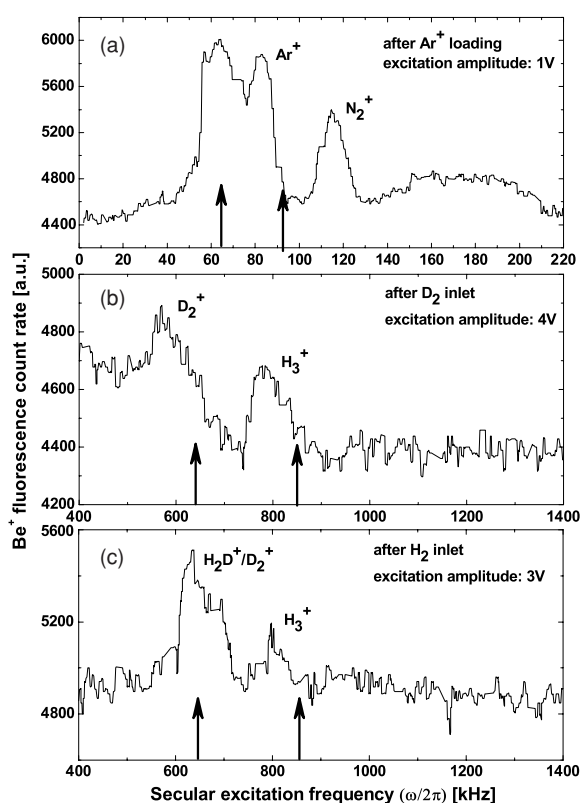
Figure 9. Motional frequency spectra for a Be$^+$ ion crystal after inlet and electron-impact ionization of Ar gas (a), after subsequent inlet of neutral D$_2$ (b), and followed by inlet of neutral H$_2$ (c). Arrows as before.

formation of mainly H$_3^+$ ions (in contrast to the experimental observation). The difference in the secular frequencies between the mass-4 features in figures 9(b) and (c) is due to the different excitation amplitudes, with the larger amplitude leading to a downward shift of the motional frequency [27].

5. Conclusion

We have demonstrated a novel production method for translationally ultracold H$_3^+$, H$_2$D$^+$ and D$_2$H$^+$ ions, based on two-step chemical reactions. The method was also used to produce samples of ultracold D$_3^+$, D$_2^+$ or D$^+$ ions. These sympathetically cooled ions were detected via excitation of their trap (secular) modes. For the interpretation of the measured secular mass spectra we used MD simulations. When the reaction chain is stopped at the first step, ultracold diatomic and triatomic molecular hydrides, e.g. ArH$^+$, ArD$^+$, N$_2$H$^+$ and N$_2$D$^+$, are obtained. The ion number in the multi-species ion crystals can be varied over a wide range from a few hundreds to several thousands, with SC particle fractions of up to 70%. Also, ion crystals containing small numbers ($<$10) of molecular hydrogen ions or their deuterated isotopomers can reliably be produced with a high degree of control. Using MD simulations we estimate the translational temperature of the crystallized molecular ions at below 20 mK.

The results described in this work could serve as systems for precision (spectroscopic) measurements on ultracold molecules. Such ultracold molecular samples in their electronic ground states could be used to perform precise tests of quantum chemical theories, to investigate chemical reactions with ultracold neutral atoms and molecules, and to implement schemes for laser manipulation of internal degrees of freedom. Reactions between cold H_3^+ ions and neutral molecular hydrogen isotopes are important for astrophysics. Furthermore, ArH^+, ArD^+ or H_3^+ ions are attractive systems for tests of time independence of particle masses. The produced two- and multi-species ion crystals could also be used to systematically study trap modes as a function of temperature and ion number.

Acknowledgments

References

[1] Fröhlich U, Roth B, Antonini P, Lämmerzahl C, Wicht A and Schiller S 2004 Ultracold trapped molecules: novel systems for test of the time-independence of the electron-to-proton mass ratio *Lecture Notes in Physics* vol 648 (Berlin: Springer) pp 297–307

[2] Vogelius I S, Madsen L B and Drewsen M 2004 Rotational cooling of heteronuclear molecular ions $^{1,2,3}\Sigma$ and $^2\Pi$ electronic ground states *Phys. Rev.* A **70** 053412

[3] Vogelius I S, Madsen L B and Drewsen M 2002 Blackbody-radiation-assisted laser cooling of molecular ions *Phys. Rev. Lett.* **89** 173003

[4] Laughlin K B, Blake G A, Cohen R C, Hoyde D C and Saykally R J 1987 Determination of the dipole moment of ArH^+ from the rotational Zeeman effect by tunable far-infrared laser spectroscopy *Phys. Rev. Lett.* **58** 996–9

[5] Schmidt P O, Rosenband T, Langer C, Itano W M, Bergquist J C and Wineland D J 2005 Spectroscopy using quantum logic *Science* **309** 749–52

[6] Herbst E 2000 The astrochemistry of H_3^+ *Phil. Trans. R. Soc.* A **358**

[7] Glenewinkel-Meyer T and Gerlich D 1997 Single and merged beam studies of the reaction $H_2^+(v = 0, 1; j = 0, 4) + H_2 \rightarrow H_3^+ + H$ *Isr. J. Chem.* **37** 343–52

[8] See, e.g., Herbst E *et al* 2000 *Phil. Trans. R. Soc.* A **358** 1774
Mikosch J *et al* 2004 Action spectroscopy and temperature diagnostics of H_3^+ by chemical probing *J. Chem. Phys.* **121** 11030–7

[9] Larson D J, Bergquist J C, Bollinger J J, Itano W M and Wineland D J 1986 Sympathetic cooling of trapped ions: a laser-cooled two-species nonneutral ion plasma *Phys. Rev. Lett.* **57** 70

[10] Bowe P, Hornekaer L, Brodersen C, Drewsen M, Hangst J S and Schiffer J P 1999 Sympathetic crystallization of trapped ions *Phys. Rev. Lett.* **82** 2071

[11] Roth B *et al* 2005 Sympathetic cooling of $^4He^+$ ions in a radiofrequency trap *Phys. Rev. Lett.* **94** 053001

[12] Bertelsen A, Jorgensen S and Drewsen M 2005 The rotational temperature of molecular ions in Coulomb crystals *Preprint* physics/0504128

[13] Blythe P, Roth B and Schiller S 2005 Production of cold trapped molecular hydrogen ions *Phys. Rev. Lett.* **95** 183002

[14] Fröhlich U, Roth B and Schiller S 2005 Ellipsoidal Coulomb crystals in a linear radiofrequency trap *Phys. Plasmas* **12** 073506

[15] Schnitzler H, Fröhlich U, Boley T K W, Clemen A E M, Mlynek J, Peters A and Schiller S 2002 All-solid-state tunable continuous-wave ultraviolet source with high spectral purity and frequency stability *Appl. Opt.* **41** 7000

[16] Raizen M G, Gilligan J M, Bergquist J C, Itano W M and Wineland D J 1992 Ionic crystals in a linear Paul trap *Phys. Rev.* A **45** 6493

[17] Baer M and Beswick J A 1979 Electronic transitions in the ion–molecule reaction $(Ar^+ + H_2 \leftrightarrow ar + H_2^+) \rightarrow ArH^+ + H$ *Phys. Rev.* A **19** 1559

[18] Bedford D K and Smith D 1990 Variable-temperature selected ion flow tube studies of the reactions of Ar^+, Ar_2^+ and ArH_n^+ (n = 1-3) ions with H_2, HD and D_2 at 300 K and 80 K *Int. J. Mass Spectrom. Ion Process.* **98** 179–90

[19] McDaniel E W, Cermak V, Dalgarno A, Ferguson E E and Friedman L 1970 *Ion–Molecule Reactions* (New York: Wiley)

[20] Huber K P and Herzberg G 1979 *Molecular Spectra and Molecular Structure* (New York: Van Nostrand-Reinhold)

[21] Bowers M T and Elleman D E 1969 Kinetic analysis of the concurrent ion–molecule reactions in mixtures of argon and nitrogen with H_2, D_2, and HD utilizing ion-ejection-ion-cyclotron-resonance techniques *J. Chem. Phys.* **51** 4606–17

[22] Roche A E, Sutton M M, Bohme D K and Schiff H I 1971 Determination of proton affinity from the kinetics of proton transfer reactions: I. Relative proton affinities *J. Chem. Phys.* **55** 5480

[23] Adams N G and Smith D 1984 A further study of the near-thermoneutral reactions $O_2H^+ + H_2 \leftrightarrow H_3^+ + O_2$ *Chem. Phys. Lett.* **105** 604

[24] Baba T and Waki I 1996 Cooling and mass-analysis of molecules using laser-cooled atoms *Japan. J. Appl. Phys.* **35** L1134

[25] Roth B, Ostendorf A, Wenz H and Schiller S 2005 Production of large molecular ion crystals via sympathetic cooling by laser-cooled Ba^+ *J. Phys. B: At. Mol. Opt. Phys.* **38** 3673–85

[26] Schiller S and Lämmerzahl C 2003 Molecular dynamics simulation of sympathetic crystallization of molecular ions *Phys. Rev.* A **68** 053406

[27] Roth B, Blythe P and Schiller S 2005 Motional resonance coupling in cold multi-species Coulomb crystals, in preparation

[28] Roth B, Blythe P, Wenz H, Daerr H and Schiller S 2006 Ion-neutral chemical reactions between ultracold, localized ions and neutral molecules with single-particle resolution *Phys. Rev.* A **73** 042712

[29] Hasegawa T and Shimizu T 2002 Resonant oscillation modes of sympathetically cooled ions in a radio-frequency trap *Phys. Rev.* A **66** 063404

[30] Baba T and Waki I 2002 Sympathetic cooling rate of gas-phase ions in a radio-frequency-quadrupole ion trap *Appl. Phys.* B **74** 375

[31] Karpas Z, Anicich V G and Huntress W T 1979 An ion cyclotron resonance study of reactions of ions with hydrogen atoms *J. Chem. Phys.* **70** 2877–81

[32] Clow R P and Futrell J H 1972 Ion–molecule reactions in isotopic hydrogen by ion cyclotron resonance *Int. J. Mass Spectrom. Ion Phys.* **8** 119–42

[33] Adams N G and Smith D 1981 A laboratory study of the reaction $H_3^+ + HD \leftrightarrow H_2D^+ + H_2$: the electron densities and the temperatures in interstellar clouds *Astrophys. J.* **248** 373–9